

# Massive Redundancy in Gradient Transport Enables Sparse Online Learning

Aur Shalev-Merin  
Independent Researcher

## Abstract

Real-time recurrent learning (RTRL) computes exact online gradients by propagating a Jacobian tensor forward through recurrent dynamics, but at  $O(n^4)$  cost per step. Prior work has sought structured approximations (rank-1 compression, graph-based sparsity, Kronecker factorization). We show that, in the continuous error signal regime, the recurrent Jacobian is *massively redundant*: propagating through a random 6% of paths ( $k=4$  of  $n=64$ ) recovers  $84 \pm 6\%$  of full RTRL’s adaptation ability across five seeds, and the absolute count  $k=4$  remains effective from  $n=64$  to  $n=256$  (6%  $\rightarrow$  1.6%, recovery  $84 \rightarrow 78\%$ ), meaning sparse RTRL becomes relatively cheaper as networks grow, with modest recovery degradation. In RNNs, the recovery is selection-invariant (even adversarial path selection works) and exhibits a step-function transition from zero to any nonzero propagation. Spectral analysis reveals the mechanism: the Jacobian is full-rank but near-isotropic (condition numbers 2.6–6.5), so any random subset provides a directionally representative gradient estimate. On chaotic dynamics (Lorenz attractor), sparse propagation is more numerically stable than full RTRL (CV 13% vs. 88%), as subsampling avoids amplifying pathological spectral modes; on non-chaotic tasks, full RTRL is stable. The redundancy extends to LSTMs ( $k=4$  matches full RTRL) and to transformers via sparse gradient transport (50% head sparsity outperforms the dense reference; 33% is borderline), with higher thresholds reflecting head specialization rather than isotropy. On real primate neural data, sparse RTRL ( $k=4$ ) adapts online to cross-session electrode drift ( $80 \pm 11\%$  recovery, 5 seeds), where sparse propagation is again more stable than full RTRL. Without continuous error signal, Jacobian propagation accumulates numerical drift and degrades all RTRL variants, a scope condition for all forward-mode methods. Results hold with SGD ( $92 \pm 1\%$  recovery on one task), suggesting independence from optimizer choice.

## 1 Introduction

Online learning in recurrent networks requires solving a credit assignment problem: how does changing a weight now affect outputs in the future? Two classical approaches bracket the design space. Backpropagation through time [BPTT; Werbos, 1990] stores a trajectory of hidden states and backpropagates through the unrolled computation graph. This is effective but fundamentally offline and memory-intensive. Real-time recurrent learning [RTRL; Williams and Zipser, 1989] propagates a Jacobian tensor forward in time, tracking how each parameter affects the current hidden state through the entire history of recurrent dynamics. RTRL is truly online (no stored trajectories, no discrete training phases), but its  $O(n^4)$  per-step cost has limited it to small networks.

Between these extremes lies a spectrum of approximations. At the cheap end, eligibility traces [Murray, 2019, Bellec et al., 2020] drop the Jacobian propagation term entirely, reducing cost to  $O(n^2)$  but losing the ability to assign credit through recurrent connections. At the expensive end, exact methods like Benzing et al. [2019] achieve  $O(n^3)$  with Kronecker structure. In between, UORO [Tallec and Ollivier, 2018] compresses the Jacobian to rank 1, SnAp [Menick et al., 2021]

exploits graph structure in weight-sparse networks, and element-wise architectures [Irie et al., 2024] eliminate inter-neuron recurrence to make RTRL tractable. Each method proposes a specific structured approximation with specific tradeoffs between cost, bias, and variance.

We ask a more basic question: **how much of the recurrent Jacobian is actually needed?** Rather than designing a new approximation scheme, we test the simplest possible one: randomly dropping most of the Jacobian propagation paths and keeping a small arbitrary subset. If this works, the information in the Jacobian is redundant, and the structured design choices in prior work may be solving a problem that does not need solving.

We find massive redundancy, in the regime where RTRL is effective (continuous, dense error signals). On dynamical prediction tasks with online distribution shifts, propagating through a random 4 out of 64 Jacobian paths (6%) recovers 78–84% of full RTRL’s adaptation ability (log-scale recovery across 5 seeds). The recovery is:

- **Robust across tasks and architectures:** sine waves, chaotic Lorenz attractors, multi-regime dynamics, and LSTMs with gate Jacobian sparsification.
- **Absolute- $k$  scaling:**  $k=4$  works at  $n=64$  (6%),  $n=128$  (3%), and  $n=256$  (1.6%), with recovery remaining substantial (78–84%) despite the fraction decreasing  $4\times$ . The required number of paths does not grow with network size, so sparse RTRL becomes relatively cheaper at larger scales.
- **Selection-invariant:** deliberately choosing the *weakest* recurrent connections works as well as choosing the strongest. Even adversarial path selection cannot break the approximation.
- **Step-function-like:** the jump from 0 paths (eligibility traces, fails) to any  $k>0$  spans two orders of magnitude. From  $k=4$  to  $k=64$  is noise.
- **Cross-architecture and cross-domain:** the redundancy extends to LSTMs ( $k=4$  matches or exceeds full RTRL through gate Jacobians), to transformers via sparse gradient transport (outperforming dense at 50% head sparsity; borderline at 33%), and to real primate neural data (80% recovery on cross-session electrode drift), with architecture-dependent thresholds explained by unit specialization.

Our contribution is empirical, not algorithmic. We do not propose sparse Jacobian propagation as a new method to be optimized. We demonstrate that gradient transport in neural networks has a structural property (massive redundancy) that makes careful optimization unnecessary, identify its mechanism in RNNs (near-isotropy of the Jacobian’s singular value spectrum), and show it extends across architectures from vanilla RNNs to LSTMs to transformers. The redundancy threshold is architecture-dependent ( $\sim 6\%$  of neurons for RNNs,  $\sim 33\%$  of attention heads for transformers), but its existence holds across all three architecture families tested. For RNNs, this reframes the RTRL approximation landscape: the bottleneck is having *any* Jacobian propagation at all, not having the *right* propagation. In transformers, where heads are specialized, selection matters more (+24.3pp Fisher oracle–anti gap), but the existence of a redundancy threshold still holds. An important scope condition bounds these results: the redundancy holds under continuous, dense error signals. On tasks with sparse supervision (copy tasks, adding problems), Jacobian propagation accumulates numerical drift and all RTRL variants, including full RTRL, degrade. The dense error signal regime is where RTRL methods have practical value, and within that regime, most of the Jacobian is unnecessary.

## 2 Background

### 2.1 Real-Time Recurrent Learning

Consider a vanilla RNN with hidden state  $h_t \in \mathbb{R}^n$ , input  $x_t$ , and output  $y_t$ :

$$h_t = \tanh(W_{hh} h_{t-1} + W_{ih} x_t + b_h) \quad (1)$$

$$y_t = W_{out} h_t + b_{out} \quad (2)$$

RTRL [Williams and Zipser, 1989] computes exact gradients in forward mode by maintaining the Jacobian tensor  $J_t[i, j, k] = \partial h_t^{(i)} / \partial \theta_{jk}$ , where  $\theta$  denotes the recurrent parameters ( $W_{hh}$ ,  $W_{ih}$ ,  $b_h$ ). The Jacobian evolves as:

$$J_t = D_t (W_{hh} J_{t-1} + B_t) \quad (3)$$

where  $D_t = \text{diag}(1 - h_t^2)$  is the derivative of  $\tanh$  and  $B_t$  contains the immediate (direct) derivatives of  $h_t$  with respect to  $\theta$ : for  $W_{hh}$ , row  $i$  of  $B_t$  is  $h_{t-1}^\top$  in the block corresponding to weight row  $i$ , and zero elsewhere.

The term  $W_{hh} J_{t-1}$  is the *Jacobian propagation term*. It captures how sensitivity to parameters ripples through recurrent connections over time, the mechanism by which RTRL assigns credit across time steps. The cost of computing this term dominates: the Jacobian tensor has  $n \times n \times |\theta_{\text{rec}}|$  entries, and the matrix-tensor contraction with  $W_{hh}$  costs  $O(n^4)$  per step for the recurrent weight group ( $n^2$  parameters, each requiring  $O(n^2)$  work).

Given  $J_t$ , the gradient of a per-step loss  $L_t = \ell(y_t, \text{target}_t)$  is:

$$\frac{\partial L_t}{\partial \theta} = \frac{\partial L_t}{\partial y_t} W_{out} J_t \quad (4)$$

This gradient is exact, online (computable at each step without stored history), and local in time (depends only on current quantities). The price is the  $O(n^4)$  Jacobian update.

### 2.2 Eligibility Traces

Eligibility traces [Murray, 2019, Bellec et al., 2020] approximate RTRL by dropping the Jacobian propagation term entirely:

$$\tilde{J}_t = D_t B_t \quad (5)$$

or, with a decay factor  $\lambda$ :

$$\tilde{J}_t = \lambda D_t \tilde{J}_{t-1} + D_t B_t \quad (6)$$

In both cases, the  $W_{hh} J_{t-1}$  term is absent. This reduces cost to  $O(n^2)$  per step but assumes that each weight only affects the hidden state at the current time step. The approximation discards all sensitivity that propagates through recurrent connections, precisely the mechanism needed for temporal credit assignment.

This is not a minor omission. Eligibility traces are equivalent to RTRL in a feedforward network (where  $W_{hh} = 0$ ). In a recurrent network, they retain only the “direct” component of the gradient and lose the “recurrent” component that carries information about how parameter changes at time  $t$  affect hidden states at times  $t+1, t+2, \dots$ . It is this recurrent component that enables adaptation to distributional shifts, as we demonstrate empirically in Section 4.

Table 1: RTRL approximation methods. All propose structured approximations with specific design tradeoffs. None tests whether unstructured random sparsification suffices.

Method	Mechanism	Cost	Constraint
UORO [Tallec and Ollivier, 2018]	Rank-1 compression	$O(n^2)$	High variance
SnAp [Menick et al., 2021]	Graph-structured sparsity	$O(n^2s)$	Weight-sparse RNN
OK [Benzing et al., 2019]	Kronecker-sum approx	$O(n^3)$	None
Element-wise [Irie et al., 2024]	Kill inter-neuron recurrence	$O(n^2)$	Architectural change
RFLO [Murray, 2019]	Drop Jacobian term	$O(n^2)$	= eligibility traces

### 2.3 Prior RTRL Approximations

Several methods approximate the Jacobian propagation term rather than dropping it entirely. Table 1 summarizes the landscape.

The closest prior work is SnAp [Menick et al., 2021], which also sparsifies the Jacobian propagation but uses graph-structured sparsity in weight-sparse RNNs. We compare in detail in Section 6.

A common thread across all prior methods is that each proposes a *specific structured approximation* with specific design choices: which rank to use (UORO), which graph distance (SnAp), which Kronecker structure (OK), which neurons to decouple (Irie). Our work asks whether any of these choices matter, and finds that they largely do not.

## 3 Method

### 3.1 Sparse Jacobian Propagation

The full RTRL update (Eq. 3) propagates sensitivity through all  $n$  recurrent connections for each neuron  $i$ :

$$J_t[i, :, :] = (1 - h_t^{(i)2}) \left( \sum_{l=1}^n W_{hh}[i, l] \cdot J_{t-1}[l, :, :] + B_t[i, :, :] \right) \quad (7)$$

We restrict the sum to a fixed random subset  $\mathcal{S}_i \subset \{1, \dots, n\}$  of size  $k$  for each neuron  $i$ :

$$\hat{J}_t[i, :, :] = (1 - h_t^{(i)2}) \left( \sum_{l \in \mathcal{S}_i} W_{hh}[i, l] \cdot \hat{J}_{t-1}[l, :, :] + B_t[i, :, :] \right) \quad (8)$$

The immediate derivative term  $B_t$  is unchanged: every neuron retains full information about how its own parameters directly affect its own activation. Only the *propagation* of sensitivity through recurrent connections is sparsified. The network weights  $W_{hh}$  remain fully dense; the network architecture and forward dynamics are identical to a standard RNN. Only the gradient computation is approximate.

**Implementation.** In practice, we construct a binary mask  $M \in \{0, 1\}^{n \times n}$  where  $M[i, l] = 1$  iff  $l \in \mathcal{S}_i$ , and compute the masked Jacobian update as:

$$\hat{J}_t = D_t \left( (W_{hh} \odot M) \hat{J}_{t-1} + B_t \right) \quad (9)$$

where  $\odot$  denotes elementwise multiplication. This replaces the  $W_{hh}J_{t-1}$  contraction in the standard einsum with  $(W_{hh} \odot M)J_{t-1}$ , zeroing out contributions from neurons outside each neuron’s selected subset.

**Subset construction.** Our default selection arranges hidden units on an arbitrary ring and assigns each neuron  $i$  the  $k/2$  neighbors on each side. Since  $W_{hh}$  is dense, this ring ordering has no relation to the network’s learned connectivity; it is a random assignment. We verify this by testing four additional selection strategies in Section 4.3, including random selection and adversarial (worst-case) selection.

### 3.2 Cost Analysis

The computational bottleneck in RTRL is the Jacobian propagation: the contraction of  $W_{hh}$  (an  $n \times n$  matrix) with  $J_{t-1}$  (an  $n \times n \times p$  tensor, where  $p$  is the number of parameters in the corresponding group). For  $W_{hh}$  itself,  $p = n^2$ , so the contraction costs  $O(n \cdot n \cdot n^2) = O(n^4)$  per step.

With sparse propagation, each row  $i$  of the contraction sums over  $k$  terms instead of  $n$ . The cost reduces to  $O(k \cdot n^3)$  per step, a factor of  $n/k$  cheaper than full RTRL. For  $k=4$  and  $n=64$ , this is a  $16\times$  reduction; for  $k=4$  and  $n=256$ , a  $64\times$  reduction. The savings scale linearly with network size because  $k$  remains fixed while  $n$  grows.

Table 2: Per-step computational cost for RTRL variants.

Method	Cost per step	Notes
Full RTRL	$O(n^4)$	Exact forward-mode gradients
Sparse RTRL ( $k$ neighbors)	$O(k \cdot n^3)$	$k \ll n$ ; dense weights
Eligibility traces	$O(n^2)$	No Jacobian propagation
UORO	$O(n^2)$	Rank-1, high variance
SnAp	$O(n^2 \cdot s)$	$s$ = propagation steps; weight-sparse

### 3.3 Evaluation Protocol: Online Adaptation

We evaluate on a task that directly tests temporal credit assignment: *online next-step prediction with mid-stream distribution shifts*. The network trains continuously on a streaming signal, receiving one input per time step and updating parameters immediately. At a predetermined point, the data distribution changes (e.g., a frequency shift in a sine wave, a parameter change in a dynamical system). We measure prediction quality before and after the shift.

This evaluation differs from standard RTRL benchmarks in the literature. Copy tasks [Hochreiter and Schmidhuber, 1997], character-level language modeling [Benzing et al., 2019], and adding problems [Hochreiter and Schmidhuber, 1997] test whether a method can learn a fixed task. Our protocol tests whether a method can *adapt* when the task changes, a more direct test of the temporal credit assignment mechanism, since adaptation requires the gradient to carry information about how the current dynamics differ from the dynamics the network was trained on.

**Gap recovery metric.** To compare methods across tasks with different MSE scales, we define *gap recovery* on a logarithmic scale. Let  $\text{MSE}_0$  denote the post-shift MSE with eligibility traces ( $k=0$ , the floor: no Jacobian propagation, no adaptation) and  $\text{MSE}_n$  denote the post-shift MSE with full RTRL ( $k=n$ , the ceiling: exact Jacobian, full adaptation). For a sparse variant with  $k$  neighbors:

$$\text{Recovery}(k) = \frac{\log \text{MSE}_0 - \log \text{MSE}_k}{\log \text{MSE}_0 - \log \text{MSE}_n} \times 100\% \tag{10}$$

A recovery of 0% means the sparse variant is no better than eligibility traces; 100% means it matches full RTRL. Intuitively, 50% recovery means the sparse variant achieves the geometric mean of the trace and full-RTRL error levels. Values above 100% indicate the sparse variant outperforms full RTRL, possible when sparsification acts as implicit regularization (Section 4.2).

## 4 Experiments

We test the redundancy of gradient transport through nine experiments, each answering one question in a logical chain: (1) does any partial Jacobian propagation recover adaptation? (2) does this hold on complex, chaotic dynamics and larger networks? (3) does the *choice* of which paths to keep matter? (4) where does it break? (5) does the redundancy extend to gated architectures? (6) does the absolute- $k$  scaling law hold at larger network sizes? (7) does an analogous redundancy extend to transformers? (8) does head selection matter in transformers? (9) does the finding transfer to real-world neural data?

Experiments 1–6 use the same core setup: an RNN with explicit parameters trained online with Adam ( $\text{lr} = 0.001$ ,  $\beta_1 = 0.9$ ,  $\beta_2 = 0.999$ ). Experiments 1–4 use a vanilla tanh RNN with dense  $W_{hh}$ ; Experiment 5 uses an LSTM; Experiment 7 uses a vision transformer on continual image classification. We evaluate on *online adaptation to distribution shifts*: the data stream changes mid-sequence (or mid-task-sequence for transformers), and we measure how well each method tracks the new distribution. This evaluation angle is distinct from standard RTRL benchmarks (which test convergence on a fixed task) and directly tests the credit-assignment mechanism we are studying. RNN experiments run on CPU in minutes; transformer experiments run on GPU. Full implementation details (hyperparameters, architectures, training schedules) are provided alongside each experiment.

**Metric.** We report gap recovery (Eq. 10) throughout; values above 100% indicate the sparse variant outperforms full RTRL.

**Implementation validation.** Our RTRL and eligibility trace implementations were validated against the independent reference implementation of Marschall et al. [2020], producing exact numerical agreement (zero difference) on both full RTRL and RFLO baselines across 2000 online steps with shared weight initialization.

### 4.1 Experiment 1: The Jacobian is Massively Redundant

How much of the recurrent Jacobian do you actually need? We test this on the simplest possible task: a 1D sine wave whose frequency shifts from 0.1 to 0.3 at  $t=1000$  in a 2000-step online stream. A vanilla RNN ( $n=64$ ) performs next-step prediction. We sweep the number of Jacobian propagation paths:  $k \in \{0, 4, 8, 16, 32, 64\}$ , where  $k=0$  is eligibility traces and  $k=64$  is full RTRL. Paths are selected as  $k/2$  contiguous neighbors on each side of an arbitrary ring ordering over hidden units.

The result is a step function. Table 3 shows that  $k=4$  (6% of hidden units) recovers  $84 \pm 6\%$  of full RTRL’s adaptation ability across 5 seeds. The jump from  $k=0$  to  $k=4$  spans two orders of magnitude in post-shift MSE ( $0.23 \rightarrow 0.0015$ ). The jump from  $k=4$  to  $k=64$  is noise.

Two features of this result are striking. First, the recovery is flat across  $k=4$  to  $k=32$ : all achieve 82–87% log-scale recovery with overlapping confidence intervals ( $\pm 3$ –6%). In absolute terms, all partial variants achieve post-shift MSE of 0.001–0.002, within a factor of 3 of full RTRL, while

Table 3: Post-shift MSE and gap recovery on sine frequency shift ( $n=64$ , 5 seeds, mean  $\pm$  s.d.). The jump from  $k=0$  to any  $k \geq 4$  spans two orders of magnitude; further increasing  $k$  adds no systematic improvement.

$k$	Fraction	Post-shift MSE	Recovery (%)
0 (traces)	0%	$0.23 \pm 0.15$	0
4	6%	$0.0015 \pm 0.0005$	$84 \pm 6$
8	12.5%	$0.0016 \pm 0.0005$	$82 \pm 5$
16	25%	$0.0017 \pm 0.0005$	$82 \pm 6$
32	50%	$0.0012 \pm 0.0002$	$87 \pm 3$
64 (full)	100%	$0.0006 \pm 0.0000$	100
BPTT $w=1$ (ref)	—	$0.0015 \pm 0.0007$	—

$k=0$  is two orders of magnitude worse. The Jacobian information needed for online adaptation is present in any small random subset of the propagation paths. Second, the BPTT reference ( $0.0015 \pm 0.0007$ ) uses per-step window-1 backpropagation and achieves MSE comparable to  $k=4$ ; both are limited by per-step credit assignment, but even this crude Jacobian propagation captures the relevant signal.

**Comparison with truncated BPTT.** In a separate ablation (3 seeds, learning rates selected per-window via sweep), we compare sparse RTRL against truncated BPTT with windows  $w \in \{1, 10, 50\}$ . Sparse RTRL ( $k=4$ ) achieves post-shift MSE of  $0.0011 \pm 0.0001$ , comparable to or better than BPTT  $w=1$  ( $0.0014 \pm 0.0009$ ) and BPTT  $w=10$  ( $0.0016 \pm 0.0019$ ), while operating fully online with  $O(1)$  temporal memory. BPTT  $w=50$  fails to converge properly (pre-shift MSE 0.021) despite learning rates being swept for all window sizes including  $w=50$ , illustrating truncated BPTT’s sensitivity to the window–learning-rate interaction, a tuning problem sparse RTRL avoids entirely. Sparse RTRL also exhibits substantially lower variance across seeds than either BPTT variant.

## 4.2 Experiment 2: Scaling to Chaotic Dynamics

Does this redundancy survive when the dynamics are genuinely complex? A sine wave is a single-frequency oscillator. We now test on the Lorenz attractor, a 3D chaotic system with nonlinear coupling between state variables. The RNN ( $n=64$ ,  $n=128$ ) predicts the next state of the Lorenz system integrated via RK4 ( $dt=0.01$ ). At  $t=2000$ , the Lorenz parameter  $\rho$  shifts from 28 to 20, qualitatively changing the attractor geometry. We also test multi-regime sine waves (4 frequency regimes, 3 shift points) to evaluate repeated adaptation.

The redundancy holds, and on chaotic dynamics, sparse Jacobian propagation is not only effective but *more numerically stable* than full RTRL. Table 4 shows post-shift MSE for  $k=4$  and full RTRL across 5 seeds at both  $n=64$  and  $n=128$ . The key finding:  $k=4$  produces tight, stable predictions across all seeds (coefficient of variation 8–13%), while full RTRL diverges on a seed-dependent fraction (CV 88–161%). At  $n=64$ , full RTRL fails on 2 of 5 seeds (post-shift MSE exceeding traces); at  $n=128$ , it fails on 3 of 5. This is consistent with sparse propagation implicitly regularizing the exponentially growing Jacobian on chaotic dynamics (see Section 5).

The scaling result is important:  $k=4$  at  $n=128$  (3.1% of hidden units) achieves post-shift MSE of  $0.016 \pm 0.001$ , nearly identical to  $k=4$  at  $n=64$  ( $0.015 \pm 0.002$ ). The required number of propagation

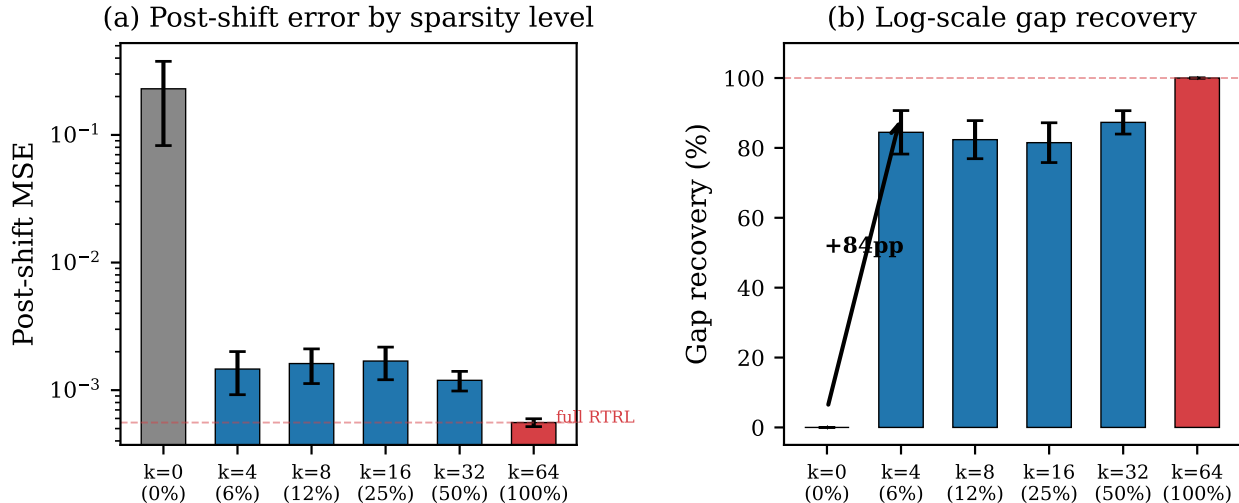


Figure 1: The Jacobian is massively redundant. (a) Post-shift MSE drops by two orders of magnitude from  $k=0$  (eligibility traces) to  $k=4$  (6% of paths), then remains flat through  $k=64$  (full RTRL). (b) Log-scale gap recovery shows a step function: any  $k \geq 4$  recovers 82–87% of full RTRL. Error bars:  $\pm 1$  s.d. across 5 seeds.

paths does not grow with network size; it is the absolute count  $k$ , not the fraction  $k/n$ , that determines performance. We confirm this scaling law up to  $n=256$  in Experiment 6 (Section 4.6).

On multi-regime sine (Table 5),  $k=4$  recovers  $80 \pm 12\%$  across 5 seeds at the first shift point, with no anomalous seeds or RTRL instability (multi-sine is non-chaotic).

**Comparison with UORO.** We compare against UORO [Tallec and Ollivier, 2018], a published rank-1 Jacobian approximation. The comparison reveals a task-dependent tradeoff. On Lorenz, UORO achieves the best post-shift MSE of any method ( $0.0025 \pm 0.0006$  across 5 seeds), outperforming both  $k=4$  ( $0.015 \pm 0.002$ ) and full RTRL ( $0.036 \pm 0.035$ ). UORO’s rank-1 compression acts as strong regularization on the exponentially growing chaotic Jacobian. On multi-regime sine (non-chaotic), UORO’s compression destroys useful gradient information: post-shift MSE of  $0.049 \pm 0.005$  (5 seeds), an order of magnitude worse than  $k=4$  ( $0.005 \pm 0.002$ ). Sparse Jacobian propagation is the more robust general-purpose approach; UORO has a niche advantage specific to chaotic dynamics where the exact Jacobian is pathological.

### 4.3 Experiment 3: Selection Does Not Matter

We have shown that a random 6% of Jacobian paths suffices. But does the *choice* of which paths to keep matter? If an oracle that selects the “best” paths significantly outperforms random selection, there is headroom for learned selection mechanisms. If even deliberately adversarial selection works, the redundancy is so complete that optimization of the selection is unnecessary.

We test five selection strategies, all at  $k=4$  on  $n=64$ :

- **Ring:** contiguous neighbors on an arbitrary ring (baseline from Experiments 1–2)
- **Random:** random  $k$  per neuron, fixed at initialization

Table 4: Post-shift MSE on Lorenz attractor (5 seeds).  $k=4$  is stable across all seeds; full RTRL diverges on chaotic dynamics. Bold values indicate failure (MSE  $>3\times$  the  $k=4$  mean).

Seed	$n=64$		$n=128$	
	$k=4$	Full RTRL	$k=4$	Full RTRL
42	0.015	0.015	0.016	<b>0.067</b>
123	0.016	0.011	0.015	0.021
7	0.018	<b>0.046</b>	0.015	<b>0.876</b>
2024	0.012	0.013	0.018	<b>0.063</b>
31337	0.014	<b>0.093</b>	0.018	0.012
Mean $\pm$ s.d.	$0.015 \pm 0.002$	$0.036 \pm 0.035$	$0.016 \pm 0.001$	$0.208 \pm 0.374$

Table 5: Post-shift MSE and gap recovery on multi-regime sine at first shift point ( $n=64$ , 5 seeds). Unlike Lorenz, full RTRL is stable on non-chaotic dynamics.

Seed	Traces	$k=4$	Full RTRL	Recovery (%)
42	0.100	0.0072	0.0022	69
123	0.178	0.0037	0.0019	85
7	0.202	0.0028	0.0020	93
2024	0.040	0.0057	0.0020	65
31337	0.100	0.0035	0.0023	89
Mean $\pm$ s.d.		$0.0046 \pm 0.0016$	$0.0021 \pm 0.0001$	$80 \pm 12$

- **Oracle** (top  $|W_{hh}|$ ): strongest recurrent connections by weight magnitude, recomputed every 200 steps
- **Anti-oracle** (bottom  $|W_{hh}|$ ): *weakest* recurrent connections, deliberately the worst choice
- **Dynamic oracle**: top  $k$  by  $|W_{hh}[i, l]| \cdot \|J[l, :, :]\|$ , recomputed per step (uses gradient information)

The result is unambiguous: selection does not matter. Table 6 shows post-shift MSE for all five strategies across 5 seeds on both tasks. On sine, all strategies achieve post-shift MSE of 0.0014–0.0019 (mean across seeds), with no strategy systematically dominating. On Lorenz, the dynamic Jacobian oracle is slightly *worst* ( $0.020 \pm 0.006$ ), suggesting that per-step reselection based on the chaotic Jacobian adds noise rather than signal.

Table 6: Post-shift MSE for five selection strategies, all at  $k=4$  ( $n=64$ , 5 seeds, mean  $\pm$  s.d.). No strategy is systematically better; the ranking changes across seeds.

Task	Ring	Random	Oracle	Anti-oracle	Dynamic
Sine	<b>.0015 <math>\pm</math> .0005</b>	.0016 $\pm$ .0006	.0016 $\pm$ .0004	<b>.0014 <math>\pm</math> .0008</b>	.0019 $\pm$ .0004
Lorenz	<b>.0149 <math>\pm</math> .0019</b>	.0156 $\pm$ .0006	.0155 $\pm$ .0021	.0164 $\pm$ .0010	.0199 $\pm$ .0063

This result suggests that designing learned or adaptive selection mechanisms for sparse Jacobian propagation may yield diminishing returns. Across 50 strategy-seed combinations (5 strategies  $\times$  5

## Lorenz attractor: sparse RTRL stabilizes chaotic dynamics

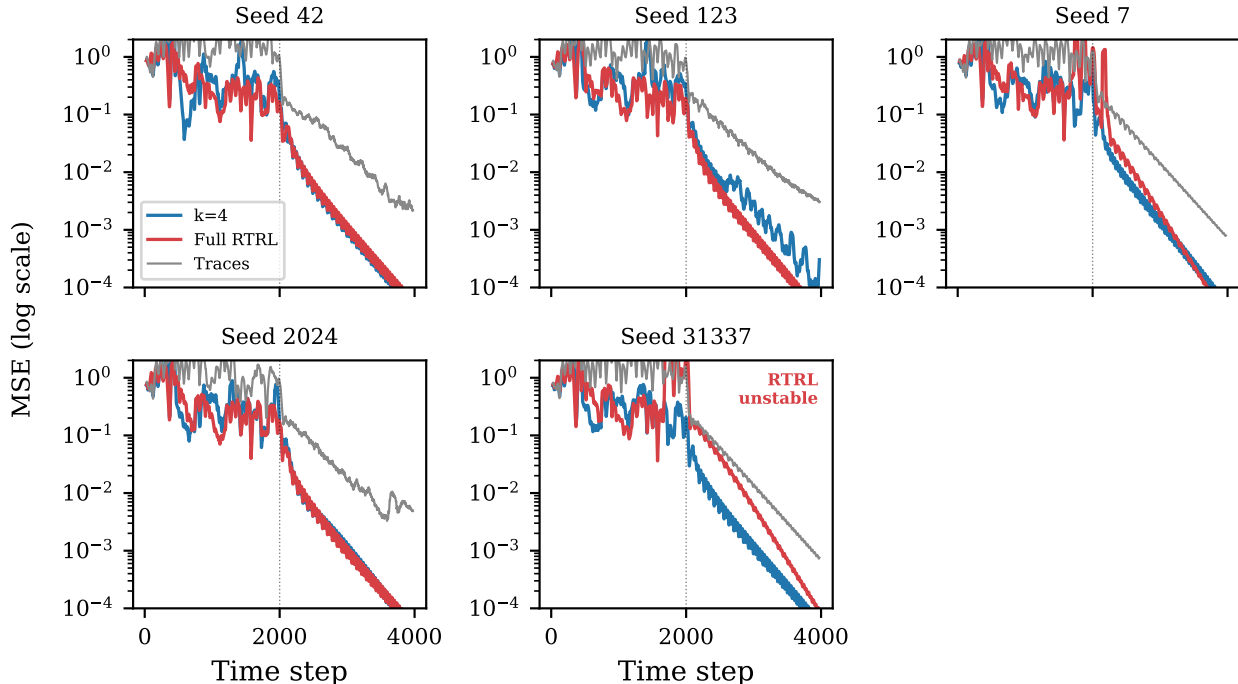


Figure 2: Sparse RTRL is more stable than full RTRL on chaotic dynamics. Per-seed loss curves on the Lorenz attractor ( $n=64$ , 5 seeds). Full RTRL (red) degrades on 2 of 5 seeds;  $k=4$  (blue) is stable on all seeds. Gray: eligibility traces ( $k=0$ ). Vertical dotted line: parameter shift at  $t=2000$ .

seeds  $\times$  2 tasks), no strategy achieves a consistent advantage. The information in the Jacobian is so redundant that any non-degenerate subset above a minimal threshold (random, structured, or adversarial) captures enough for adaptation. The design choice that matters is not *which* paths to keep, but *how many*, and the answer from Experiment 1 is: surprisingly few.

### 4.4 Experiment 4: When Forward-Mode Breaks Down

All experiments so far use tasks with continuous error signals: the network receives prediction error at every time step, and the Jacobian is grounded by gradient updates throughout the sequence. What happens when error is sparse?

We test two standard RTRL benchmarks: the *copy task* [Hochreiter and Schmidhuber, 1997] (memorize and reproduce a symbol sequence across a delay, cross-entropy loss only on output phase) and the *adding problem* [Hochreiter and Schmidhuber, 1997] (identify two marked values in a 50-step sequence, MSE loss only at the final step). Both tasks provide error signal at a fraction of time steps, leaving the Jacobian to propagate for extended periods without corrective feedback.

The result reveals a failure mode of RTRL itself, independent of sparsification. Table 7 shows that full RTRL ( $k=64$ ) is the *worst* method on both tasks, worse than BPTT, worse than eligibility traces. On the adding problem, full RTRL achieves MSE of 0.289, compared to the trivial baseline of 0.167 (predicting the expected sum of two uniform random variables).

Table 7: Standard RTRL benchmarks with vanilla tanh RNN ( $n=64$ ). No method succeeds; full RTRL is worst on both tasks. The architecture cannot solve these tasks regardless of training method.

Method	Copy T=5 (accuracy $\uparrow$ )	Adding T=50 (MSE $\downarrow$ )
Trivial baseline	0.125 (chance)	0.167 (predict mean)
BPTT	0.289	0.189
$k=0$ (traces)	0.239	0.284
$k=4$	0.239	0.281
$k=8$	0.292	0.278
$k=64$ (full RTRL)	0.130	<b>0.289</b> (worst)

Two distinct phenomena contribute to this result. First, the vanilla tanh RNN lacks the gating mechanisms needed for discrete memory tasks; these benchmarks were designed to motivate LSTMs [Hochreiter and Schmidhuber, 1997], and published methods that succeed on them use GRU or LSTM architectures [Menick et al., 2021, Tallec and Ollivier, 2018]. No gradient method can overcome an architecture that cannot maintain discrete states through tanh contraction. This makes the experiment uninformative for comparing gradient approximations: there is no gap between traces and full RTRL to measure.

Second, and more interesting: full RTRL is the *worst* method, underperforming even eligibility traces. Jacobian propagation without continuous error feedback is actively harmful. Without per-step gradient corrections, the Jacobian tensor accumulates numerical drift over  $T$  steps of ungrounded propagation, producing gradient estimates that are worse than the crude trace approximation. This failure mode predicts that RTRL-based methods will struggle on any task with sparse or delayed reward signals, a significant scope condition for the entire family of forward-mode approaches, not only for our sparse variant.

#### 4.5 Experiment 5: The Redundancy Extends to LSTMs

Experiments 1–3 establish Jacobian redundancy in vanilla tanh RNNs, where the recurrent weight matrix  $W_{hh}$  is the sole path for temporal credit assignment. LSTMs provide a qualitatively different architecture: the cell state acts as a nearly linear highway through time, with gating mechanisms controlling information flow. Does the cell state highway eliminate the need for Jacobian propagation through the gates, or does the redundancy property persist?

We test an LSTM ( $n=64$ ) with explicit gate Jacobians for RTRL. The cell state Jacobian is element-wise (diagonal) and always computed exactly; it requires no sparsification. We sparsify only the inter-neuron gate Jacobians: how gate activations at one neuron propagate sensitivity through connections to other neurons. This is the LSTM analogue of sparsifying  $W_{hh}$  in the vanilla RNN. The task is sine frequency shift ( $0.1 \rightarrow 0.3$ ), with a longer sequence ( $T=4000$ , shift at  $t=2000$ ) to ensure the LSTM converges before the shift.<sup>1</sup>

The result matches the vanilla RNN pattern (Table 8). Eligibility traces fail on 4 of 5 seeds

<sup>1</sup>An initial run with  $T=2000$  (shift at  $t=1000$ ) produced an inverted gap where traces appeared to match full RTRL. This was a convergence artifact: with insufficient pre-training, all methods were still learning the initial distribution when the shift occurred, making the post-shift comparison meaningless. Doubling the pre-training time resolved the artifact and revealed the pattern reported here. We include this as a cautionary note: verifying pre-shift convergence is essential before interpreting adaptation results.

Table 8: LSTM gate Jacobian sparsification on sine frequency shift ( $n=64$ ,  $T=4000$ , shift at  $t=2000$ , 5 seeds). The vanilla RNN pattern holds: traces fail,  $k=4$  recovers near-full RTRL performance. Seed 123 excluded from recovery (inverted gap; traces converge better than full RTRL on that seed).

Seed	Traces	$k=4$	Full RTRL	Notes
42	0.508	0.004	0.002	Clean
123	0.002	0.001	0.015	Inverted
7	0.548	0.003	0.015	$k=4$ beats full
2024	0.220	0.001	0.0002	Clean
31337	0.090	0.001	0.004	$k=4$ beats full
Mean $\pm$ s.d.		$0.002 \pm 0.001$	$0.007 \pm 0.006$	

(post-shift MSE 0.09–0.55), two orders of magnitude worse than  $k=4$ .<sup>2</sup> Sparse gate Jacobian propagation with  $k=4$  achieves post-shift MSE of  $0.002 \pm 0.001$  across all 5 seeds, comparable to or better than full RTRL ( $0.007 \pm 0.006$ ). On 2 of 5 seeds,  $k=4$  outperforms full RTRL, the same sparse regularization effect observed on the Lorenz attractor.

The cell state highway does not eliminate the need for gate Jacobian propagation. Despite providing a linear gradient path through time, the LSTM still requires inter-neuron sensitivity information flowing through the gates, and this information exhibits the same redundancy as in vanilla RNNs. As with Lorenz,  $k=4$  is more numerically stable than full RTRL: CV of 69% vs 88%.

We also tested the LSTM on the Lorenz attractor (with extended pre-training,  $T=8000$ , shift at  $t=4000$ ). LSTM RTRL did not converge to acceptable pre-shift performance on chaotic dynamics: pre-shift MSE remained 0.08–0.90 across all methods and seeds, compared to 0.01–0.05 for the vanilla RNN. This affects full RTRL as well as sparse variants, and is consistent with the theoretical result of Mikhaeil et al. [2022] that loss gradients of recurrent networks producing chaotic dynamics always diverge, regardless of architecture (their result covers all first-order Markovian recursive maps, including LSTMs and GRUs). We conjecture that the LSTM’s four-gate structure compounds rather than ameliorates this instability. The LSTM redundancy finding is therefore established on smooth dynamics (sine) but inconclusive on chaotic dynamics.

This result upgrades the redundancy finding from architecture-specific to architecture-general on smooth dynamics. The bottleneck for online adaptation is having *any* Jacobian propagation through the gates, not having the right propagation, and not the cell state highway alone.

#### 4.6 Experiment 6: Scaling to $n=256$

Experiments 1–2 established the absolute- $k$  scaling law at  $n=64$  and  $n=128$ : the number of Jacobian paths needed for adaptation does not grow with network size. We now test whether this holds at  $n=256$ , where  $k=4$  represents just 1.6% of neurons, and at  $n=512$  (0.8%), where the computational savings of sparse RTRL become substantial ( $64\times$  and  $128\times$  respectively).

At  $n=256$ , sparse propagation ( $k=4$ ) achieves consistent post-shift MSE of  $0.0038 \pm 0.0008$  across all 5 seeds (Table 9). Full RTRL shows  $22\times$  variance across seeds (0.0003–0.0065), with seed 31337 partially failing to adapt, consistent with the instability pattern observed on chaotic

<sup>2</sup>Seed 123 is anomalous: traces achieve 0.002 post-shift (better than full RTRL at 0.015), producing an inverted gap. Neither method converged well pre-shift on this seed; the trace approximation happened to suit the post-shift distribution.

Table 9: Scale test results at  $n=256$  (sine frequency shift, 5 seeds).  $k=4$  at 1.6% recovers  $78 \pm 20\%$  of the log-space gap. Seed 31337:  $k=4$  outperforms full RTRL (recovery  $>100\%$ ), another stability win consistent with the Lorenz findings.

Seed	$k=4$ post-shift MSE	$k=256$ (full)	Recovery (%)
42	0.0036	0.0003	66
123	0.0054	0.0003	62
7	0.0036	0.0010	80
2024	0.0034	0.0003	68
31337	0.0032	0.0065	116
Mean $\pm$ s.d.	$0.0038 \pm 0.0008$		$78 \pm 20$

dynamics at smaller scales. The recovery variance ( $78 \pm 20\%$ ) inherits this instability from the full RTRL ceiling;  $k=4$  absolute performance is scale-stable. Traces remain at  $\sim 0.51$  across all seeds (two orders of magnitude worse than  $k=4$ ). Spectral analysis at  $n=256$  (Table 13) confirms that the Jacobian remains near-isotropic ( $r_{95}/n = 92.5\%$ , condition number  $2.97 \pm 0.33$ , actually better conditioned than at  $n=64$  or  $n=128$ ). The recovery variance increase despite improving isotropy suggests that numerical precision, not spectral structure, is the limiting factor at larger scales.

The scaling law across all tested network sizes is:

$n$	$k=4$ fraction	$k=4$ MSE	Recovery	Seeds	Task
64	6.25%	$0.0015 \pm 0.0005$	$84 \pm 6\%$	5	Sine
128	3.13%	$0.016 \pm 0.001$	stable <sup>†</sup>	5	Lorenz
256	1.56%	$0.0038 \pm 0.0008$	$78 \pm 20\%$	5	Sine

<sup>†</sup>Full RTRL diverges on 2/5 seeds;  $k=4$  is stable on all 5 (CV 13%).

The fraction  $k/n$  decreases by  $4\times$  from  $n=64$  to  $n=256$ , while  $k=4$  absolute performance degrades modestly ( $0.0015 \rightarrow 0.0038$ ). Full RTRL degrades catastrophically: from stable at  $n=64$  to  $22\times$  seed-dependent variance at  $n=256$ . The practical reliability gap between sparse and full propagation *widens* as  $n$  grows.

At  $n=512$ , two distinct failure modes emerge. First, *numerical divergence*: on sine, full RTRL ( $k=512$ ) diverges on 1 of 2 tested seeds (post-shift MSE 1.8, far worse than eligibility traces and BPTT), while converging normally on the other. The Jacobian tensor at this scale ( $(512, 512, 512)$ , comprising 134 million floating-point entries) accumulates numerical errors through 2000 steps of repeated matrix-tensor contractions, causing the sensitivity estimates to blow up. Second, *overparameterization*: a 512-dimensional network has far more capacity than these tasks require, so local per-step updates suffice without temporal credit assignment. On Lorenz at  $n=512$  (with full RTRL skipped due to computational cost), eligibility traces achieve near-perfect performance on some seeds (post-shift MSE  $3 \times 10^{-6}$  on seed 123), while Jacobian propagation actively hurts, injecting noise from a numerically unstable tensor into a problem that does not require it. These two failure modes bound the absolute- $k$  scaling law from above: it holds up to the point where either the Jacobian becomes too large to propagate stably, or the task no longer requires temporal credit assignment due to overparameterization. This establishes  $n \approx 256\text{--}512$  as the practical ceiling for forward-mode Jacobian propagation with standard floating-point arithmetic on these tasks.

## 4.7 Experiment 7: Extension to Transformers

Experiments 1–6 establish gradient transport redundancy in recurrent architectures (vanilla RNNs and LSTMs), where the Jacobian propagation term  $W_{hh}J_{t-1}$  is the mechanism under study. Does the same redundancy principle extend to fundamentally different architectures? In transformers [Vaswani et al., 2017], the structural analogue is *sparse gradient transport*: restricting gradient flow through a subset of attention heads during backpropagation while maintaining the full forward pass.

**Mechanism.** In standard multi-head attention [Vaswani et al., 2017], the output is  $y = W_O [\text{head}_1; \dots; \text{head}_H]$ . In sparse gradient transport, all  $H$  heads compute their attention and contribute to the output projection normally. During backpropagation, non-selected heads are *detached* from the computation graph:

$$y = W_O [\tilde{h}_1; \dots; \tilde{h}_H], \quad \tilde{h}_i = \begin{cases} \text{head}_i & \text{if } i \in S \\ \text{sg}(\text{head}_i) & \text{otherwise} \end{cases} \quad (11)$$

where  $S$  is a random subset of  $k$  heads (resampled each forward pass) and  $\text{sg}(\cdot)$  denotes stop-gradient. Note that  $S$  is resampled stochastically, unlike the RNN experiments where the mask  $M$  is fixed at initialization. This stochastic selection is closer to dropout-style regularization and may contribute to the observed generalization benefit at  $k=6$ . The forward computation uses all heads; only gradient transport is restricted to  $k$  paths.

**Setup.** We use a vision transformer [Dosovitskiy et al., 2021] on Split CIFAR-10 (5 sequential tasks of 2 classes each), a standard continual learning benchmark [Zenke et al., 2017]. The model uses  $H=12$  heads (embed\_dim=192, head\_dim=16, depth=4) with a class-balanced replay buffer (1000 samples,  $\lambda=5.0$ ). Sparse gradient transport is applied to all transformer blocks. We sweep  $k \in \{1, 2, 4, 6\}$  across 3 seeds, with recovery computed as  $(\text{Acc}_{\text{sparse}} - \text{Acc}_{\text{degenerate}})/(\text{Acc}_{\text{dense}} - \text{Acc}_{\text{degenerate}})$ .

Table 10: Sparse gradient transport on Split CIFAR-10 ( $H=12$  heads, 3 seeds). All heads contribute to the forward pass; gradient flows through only  $k$  heads. At  $k=6$  (50%), sparse transport *outperforms* the dense reference (regularization effect). The threshold for  $>70\%$  recovery is  $\sim 33\%$  of heads, higher than RNNs ( $\sim 6\%$ ), reflecting greater head specialization.

Method	$k/H$	Avg Accuracy				Mean	Recovery
		Seed 42	Seed 43	Seed 44			
bptt_ref	12/12	0.407	0.397	0.374	0.393	—	
dense_ref	12/12	0.403	0.389	0.401	0.398	100%	
sparse $k=6$	6/12	0.406	0.382	0.415	0.401	107%	
sparse $k=4$	4/12	0.387	0.376	0.384	0.383	77%	
sparse $k=2$	2/12	0.353	0.325	0.336	0.338	8%	
trace_like	1/12	0.328	0.317	0.346	0.330	0%	

The results (Table 10) reveal gradient transport redundancy in transformers with a threshold between 17% and 50% of heads. At  $k=6$  (50%), sparse transport achieves 107% recovery, *outperforming* the dense reference via implicit regularization. At  $k=4$  (33%), recovery is 77% across 3 seeds (per-seed: 80%, 82%, 69%), but 2 additional seeds show compressed or inverted dense-trace

gaps (dense  $\leq$  trace), making recovery metrics unreliable and indicating that  $k=4$  is genuinely borderline. Below the threshold, performance degrades rapidly:  $k=2$  (17%) achieves only 8% recovery.

The mechanism differs from RNNs. In RNNs, the Jacobian is near-isotropic and any random subset is representative (Section 5). In transformers, attention heads are functionally specialized [Voita et al., 2019], where each learns distinct attention patterns, so gradient signal is concentrated in a subset of heads. Redundancy arises not from isotropy but from the fact that a random sample of 4–6 of 12 heads is likely to include enough of the important ones. This predicts (and Experiment 8 confirms) that head selection *should* matter in transformers, unlike in RNNs.

**Comparison with sparse forward transport.** We also test a variant where non-selected heads are *zeroed* in the forward pass rather than detached, affecting both forward computation and gradient flow (analogous to structured head dropout). This yields a higher apparent threshold of  $\sim 50\%$  for  $>70\%$  recovery. The difference quantifies forward-pass corruption: with zeroing, the degenerate baseline drops much further (accuracy 0.14 vs 0.33 with detach), creating a larger gap but one that conflates feature corruption with gradient information. The 17 percentage point threshold reduction ( $50\% \rightarrow 33\%$ ) from isolating the gradient-only effect demonstrates that the true gradient redundancy threshold is lower than naive forward sparsification suggests.

**Forgetting reduction.** Sparse gradient transport substantially reduces catastrophic forgetting. At  $k=6$ , average forgetting is 0.22 versus 0.45 for the dense reference, a  $\sim 50\%$  reduction. This regularization effect is consistent across sparsity levels and across both sparse gradient and sparse forward transport variants.

## 4.8 Experiment 8: Head Selection Matters in Transformers

In RNNs, the choice of which  $k$  Jacobian paths to propagate does not matter (Section 4.3): oracle, random, and adversarial selection all achieve equivalent recovery. Does the same hold for transformer heads?

We test this using Fisher information to identify the most and least important attention heads. After training on task 1 (the first 2-class split), we compute per-head Fisher importance by decomposing the squared gradient of the classification loss across heads in each layer’s  $W_Q$ ,  $W_K$ ,  $W_V$ , and  $W_O$  parameters. We then compare three selection strategies for tasks 2–5, all at  $k=6$  of  $H=12$ :

- **Oracle** (top-6 Fisher): select the 6 most important heads
- **Random**: select 6 heads uniformly at random (resampled each forward pass)
- **Anti-oracle** (bottom-6 Fisher): deliberately select the 6 *least* important heads

The result is consistent across seeds: head selection matters in transformers, and the signal is in gradient importance, not activation patterns (Table 11). Fisher oracle selection achieves 95.3% mean recovery while Fisher anti-oracle achieves only 71.0%, a gap of +24.3pp that is positive on all 5 seeds (+26.8, +34.3, +24.0, +25.5, +10.8pp). This is the *opposite* of the RNN finding: a Fisher-based oracle experiment in RNNs (3 seeds) yields a gap of only  $-0.6$ pp (Fisher oracle 78.8% vs. anti 79.4%), with both underperforming random selection (88.7%). Fisher importance varies up to  $1000\times$  across neurons yet carries no useful selection signal, confirming Jacobian isotropy.

Entropy-based selection, which ranks heads by how peaked their attention is (effectively selecting the most “active” heads), performs no better than random (76.4% vs. 77.5%). This rules out a dormancy-based explanation of the Fisher gap. If Fisher oracle were merely selecting active heads

Table 11: Head selection strategies on Split CIFAR-10 ( $H=12$ ,  $k=6$ , 5 seeds). Fisher oracle selects heads with the highest squared-gradient importance; entropy oracle selects heads with the lowest attention entropy (most peaked attention, i.e., least dormant). The Fisher oracle–anti gap of +24.3pp contrasts sharply with RNNs (−0.6pp; see text), while entropy oracle  $\approx$  random shows dormancy-based selection adds no useful signal. Seed 2024 is an outlier (Fisher anti recovery 88.3%); the remaining 4 seeds show gaps of +25–34pp.

Method	Recovery (%)					Mean
	Seed 7	Seed 42	Seed 43	Seed 44	Seed 2024	
Fisher oracle (top-6)	96.9	97.6	93.7	89.2	99.1	95.3
Entropy oracle (top-6)	58.0	70.0	76.9	87.8	89.5	76.4
Random	84.0	84.2	66.3	80.6	72.5	77.5
Entropy anti (bottom-6)	82.3	61.1	82.8	66.9	85.3	75.7
Fisher anti (bottom-6)	70.1	63.3	69.7	63.7	88.3	71.0

over dormant ones, entropy oracle would show a comparable advantage; it does not. The Fisher–entropy oracle gap of +18.9pp (mean across 5 seeds; per-seed range +1.4 to +38.9pp) confirms that Fisher importance captures genuine gradient specialization (which heads carry disproportionate gradient signal for adaptation) beyond what activation-based measures detect. Head dormancy is transient: by later tasks, nearly all selected heads are active, indicating that the dormancy observed at initialization resolves during training.

This confirms the prediction from Section 4.7: because transformer heads are specialized rather than isotropic, selection matters, the opposite of the RNN finding (−0.6pp Fisher gap, Section 4.3).

This finding is distinct from the head pruning literature [Voita et al., 2019, Michel et al., 2019], which asks which heads can be removed *post-training* without degrading accuracy. We ask a different question: which heads carry useful gradient signal *during training* for adaptation to distribution shifts. The Fisher oracle–anti gap demonstrates that gradient importance computed after task 1 predicts gradient utility on subsequent tasks, connecting head specialization to gradient transport redundancy across task boundaries.

**Fisher timing sensitivity.** We test the robustness of Fisher selection by expanding to 5 seeds (42–46) and comparing Fisher computed at different task boundaries. Fisher importance computed after task 1 yields  $81.6 \pm 4.0\%$  recovery on tasks 3–5 (+22.5pp oracle–anti gap), but Fisher computed after task 2 degrades to  $45.5 \pm 7.1\%$  on the same tasks, *worse* than random selection (50.9%). Early Fisher (after task 1) captures general head importance before task-specific specialization sets in; later Fisher overfits to the most recent distribution. Head importance rankings are statistically correlated across tasks (Spearman  $\rho = 0.78$ ), but small rank shifts near the selection threshold change which heads are chosen. This timing sensitivity is a limitation of Fisher-guided selection, not of the underlying redundancy finding; random selection remains robust regardless of timing.

## 4.9 Experiment 9: Cross-Session Neural Decoding

Experiments 1–8 establish gradient transport redundancy on synthetic dynamical tasks and image classification benchmarks. Does the finding transfer to real-world distribution shifts? We test on brain-computer interface (BCI) neural decoding, where electrode drift between recording sessions degrades decoder performance, a clinically significant problem that currently requires manual recalibration.

**Setup.** We use the Indy reaching dataset [O’Doherty et al., 2017, Makin et al., 2018]: 96-channel Utah array recordings from a macaque performing a center-out reaching task. We select two sessions separated by 7 months (session A: June 2016, session B: January 2017) to maximize electrode drift. Neural activity is reduced to 40 PCA dimensions (fit on session A only) and z-scored using session A statistics; session B data is processed with session A’s transform, so any distributional shift from electrode drift is preserved. A vanilla RNN decoder ( $n=64$ , same architecture and optimizer as Experiments 1–6) is trained on session A using each gradient method, then evaluated in a single online pass through session B with no recalibration. The frozen baseline uses the session-A-trained model without adaptation.

**Recovery metric.** For BCI, we define recovery relative to the frozen decoder’s degradation rather than using Eq. 10:

$$\text{Recovery}_{\text{BCI}} = \frac{\text{MSE}_{\text{frozen}}^B - \text{MSE}_{\text{method}}^B}{\text{MSE}_{\text{frozen}}^B - \text{MSE}_{\text{frozen}}^A} \times 100\% \quad (12)$$

where  $\text{MSE}_{\text{frozen}}^A$  is the frozen model’s end-of-session-A performance (the target) and  $\text{MSE}_{\text{frozen}}^B$  is its degraded session-B performance (the floor). This measures what fraction of the drift-induced degradation each method recovers through online adaptation. Note that this metric is not directly comparable to the log-scale gap recovery in Eq. 10: “80% recovery” on BCI and “84% recovery” on sine measure different quantities.

Table 12: Cross-session neural decoding (7-month electrode drift,  $n=64$ , 5 seeds). Frozen decoder degrades massively (+0.29–0.47 MSE). Sparse RTRL ( $k=4$ ) recovers  $80 \pm 11\%$  of the drift gap, with lower variance than full RTRL. Full RTRL is unstable on 2 of 5 seeds (bold), reproducing the pattern from chaotic dynamics (Table 4).

Method	Late session B MSE				
	Seed 42	Seed 123	Seed 31337	Seed 7	Seed 2024
Frozen (no adapt.)	0.734	0.547	0.674	0.628	0.580
$k=0$ (traces)	0.479	0.360	0.432	0.464	0.423
$k=4$ (6%)	0.400	0.328	0.386	0.306	0.360
$k=64$ (full RTRL)	0.303	<b>0.406</b>	0.390	0.347	<b>0.466</b>
BPTT (ref)	0.351	0.329	0.330	0.317	0.333
$k=4$ recovery	71.1%	75.6%	85.2%	97.5%	72.4%

Sparse RTRL adapts to real cross-session electrode drift (Table 12). With  $k=4$  (6% of neurons), recovery is  $80 \pm 11\%$  across 5 seeds, all seeds above the 60% threshold. The frozen decoder degrades by +0.29 to +0.47 MSE, confirming substantial electrode drift. Sparse RTRL closes most of this gap through purely online adaptation, with no recalibration step and no stored session-B data.

The stability advantage of sparse over full RTRL reappears on real neural data. Full RTRL fails on 2 of 5 seeds (recovery 48.9% and 37.6%), while  $k=4$  is stable on all 5 (recovery 71–98%). The variance pattern matches the Lorenz finding (Section 4.2):  $k=4$  Late-B MSE standard deviation is 0.037 versus 0.060 for full RTRL. On real biological signals, as on chaotic dynamics, the exact Jacobian is less reliable than a sparse approximation.

Eligibility traces ( $k=0$ ) partially adapt on BCI data (58.5% mean recovery), unlike on synthetic tasks where traces fail entirely. BCI electrode drift is slower and smoother than the abrupt frequency shifts in Experiments 1–2, allowing even crude one-step gradient estimates to track some of the

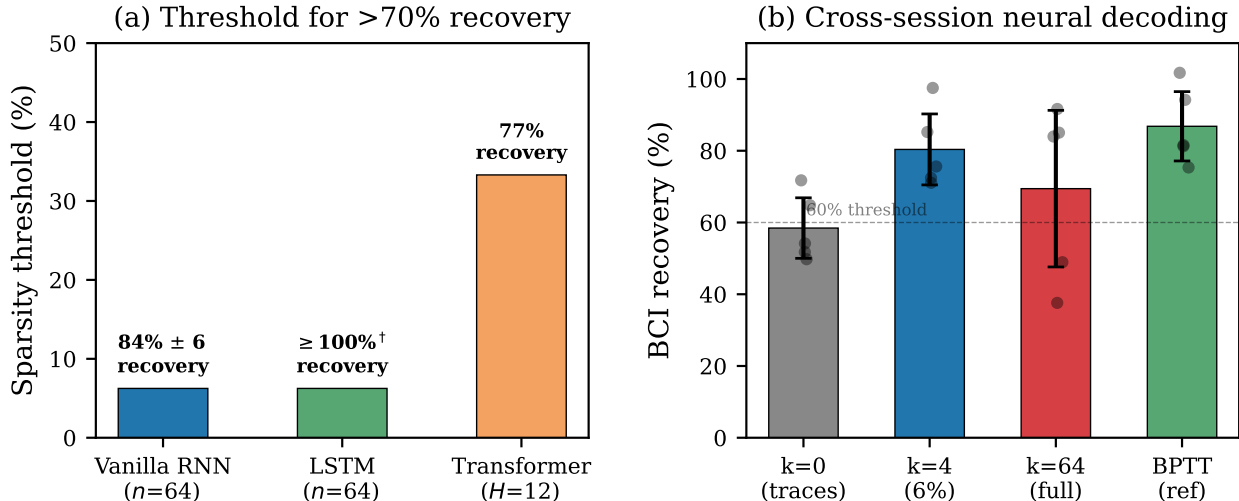


Figure 3: Gradient transport redundancy across architectures and real neural data. (a) Recovery threshold comparison: RNNs require  $\sim 6\%$  of neurons, transformers  $\sim 33\text{--}50\%$  of heads, reflecting isotropy vs. specialization. (b) BCI cross-session adaptation:  $k=4$  sparse RTRL adapts to 7-month electrode drift while the frozen decoder degrades and full RTRL is unstable on 2/5 seeds.

distributional change. However,  $k=4$  still outperforms traces by +22pp, confirming that Jacobian propagation provides substantial value even when the drift is gradual.

## 5 Discussion

### 5.1 Why is the Jacobian Redundant?

The central empirical finding of this paper, that random sparse Jacobian propagation recovers nearly all of full RTRL’s adaptation ability, demands an explanation. A natural hypothesis is that the Jacobian tensor is low-rank along the neuron axis: if the effective rank is  $r \ll n$ , then any  $k \geq r$  random samples would span the relevant subspace, explaining why  $k=4$  suffices.

We tested this by computing the singular value decomposition of the Jacobian tensor  $J_t$ , reshaped from  $(n, n, n)$  to  $(n, n^2)$ , at regular intervals during training. The low-rank hypothesis is decisively rejected: at  $n=64$ , the effective rank at the 95% variance threshold is  $r_{95} \approx 60$ ; the Jacobian is essentially full rank. At  $n=128$ ,  $r_{95} \approx 119$ . The Jacobian does not concentrate sensitivity in a low-dimensional subspace.

However, the spectral analysis reveals a different and more explanatory property: the Jacobian is *near-isotropic*. The condition number (ratio of largest to smallest singular value) is remarkably small, between 2.6 and 6.5 across all tasks and seeds (Table 13). The singular values are nearly uniform, meaning all neurons carry sensitivity information of similar magnitude. There are no privileged directions. This isotropy is not an initialization artifact: tracking condition numbers through training on the sine task ( $n=64$ , 5 seeds) shows they remain in the range 1.9–5.0 from  $t=500$  through  $t=1950$ , increasing modestly in late training (mean 2.9 at the shift point, 3.9 at  $t=1950$ ) as the network develops some directional structure, but never approaching the regime ( $>10$ ) where random subsampling would degrade. Effective rank ( $r_{95} \approx 60/64$ ) is stable throughout.

The 5-seed spectral data also reveals why full RTRL diverges on certain Lorenz seeds: the 2

Table 13: Spectral analysis of the Jacobian tensor along the neuron axis. The Jacobian is full-rank but near-isotropic: condition numbers of 2.6–6.5 indicate nearly uniform singular values. Values are mean  $\pm$  s.d. where multiple seeds are available.

Task	$n$	Seeds	$r_{95}$	Cond. ( $\sigma_1/\sigma_n$ )
Sine	64	5	$59.8 \pm 0.4$	$3.97 \pm 0.81$
Lorenz	64	3 <sup>†</sup>	$56.3 \pm 0.5$	$2.95 \pm 0.36$
Sine	128	5	$117.6 \pm 0.5$	$6.51 \pm 0.26$
Sine	256	3	$236.7 \pm 0.4$	$2.97 \pm 0.33$

<sup>†</sup>3 of 5 seeds; 2 seeds diverged (condition number  $> 10^4$ ; see text).

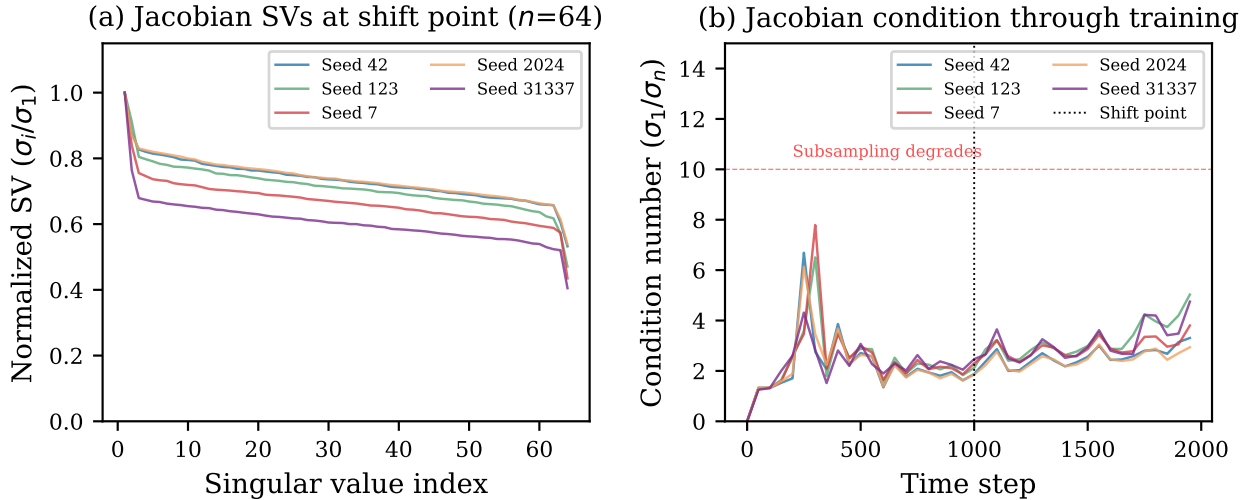


Figure 4: The Jacobian is full-rank and near-isotropic. (a) Singular value spectrum of the Jacobian tensor (reshaped to  $n \times n^2$ ) at the shift point ( $n=64$ , sine task), showing nearly uniform singular values (condition number  $\sim 4$ ). Individual seeds shown. (b) Condition number remains low (2–5) throughout training across all 5 seeds, confirming isotropy is not an initialization artifact. Red dashed line: condition = 10, above which random subsampling would degrade.

seeds where full RTRL failed (Table 4, seeds 7 and 31337 at  $n=64$ ) are exactly the seeds where the Jacobian spectrum collapses, with condition numbers exceeding  $10^4$ . On these seeds, the Jacobian loses its isotropy, concentrating sensitivity into a few dominant singular values. Full RTRL faithfully propagates this pathological spectrum; sparse propagation, by subsampling, avoids amplifying the dominant modes.

Isotropy is consistent with all features of our RNN experimental results:

- **$k=0$  fails:** with no propagation, there is no recurrent sensitivity information at all.
- **$k=4$  works:** any random sample from a near-isotropic distribution yields a gradient estimate that preserves direction. Gradient magnitudes at  $k=4$  are comparable to full RTRL (median ratio  $\approx 1.0$ ), so magnitude compensation is unnecessary, confirmed by an SGD ablation achieving  $92 \pm 1\%$  recovery across 5 seeds (see Limitations for details).
- **$k=4$  to  $k=64$  is flat:** additional samples from an isotropic source add magnitude but no new

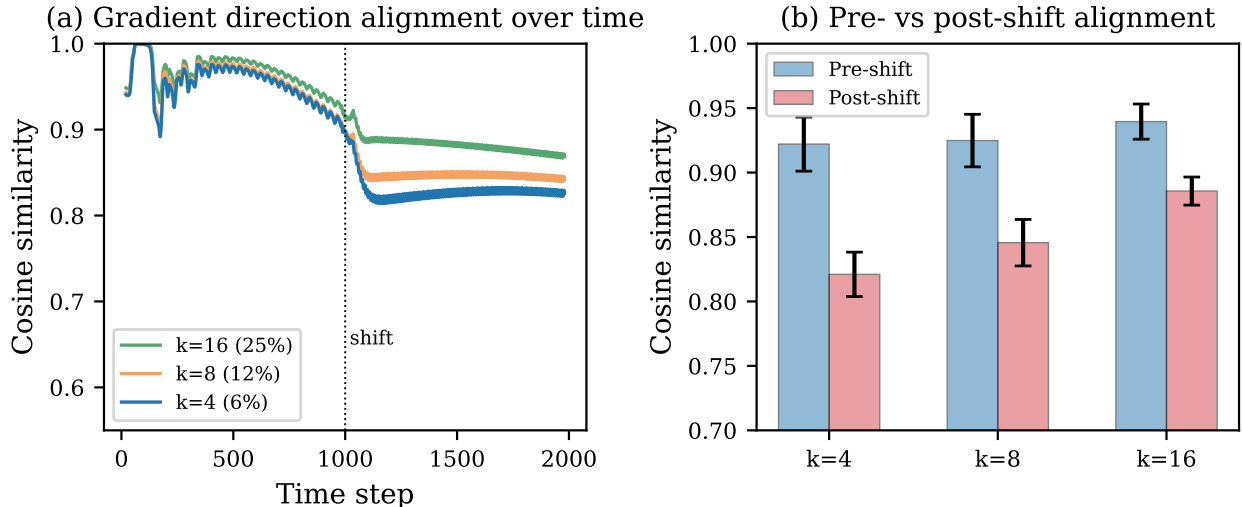


Figure 5: Sparse gradients are directionally aligned with full RTRL gradients. (a) Cosine similarity between  $k$ -sparse and full RTRL gradients over time (5-seed mean  $\pm$  s.d.). Pre-shift cosine is  $\sim 0.92$ ; post-shift dip to  $\sim 0.82$  at  $k=4$  reflects the harder adaptation regime but never collapses. (b) Post-shift cosine increases monotonically with  $k$ , consistent with the flat recovery curve.

directional information.

- **Selection does not matter:** when all singular values are similar, no subset is privileged; there are no important directions to miss.

Direct gradient measurement confirms this: cosine similarity between  $k=4$  and full RTRL gradients is  $0.92 \pm 0.02$  pre-shift and  $0.82 \pm 0.02$  post-shift (5 seeds), with a magnitude ratio of  $\sim 0.84$ . Even during rapid adaptation after a distribution shift, sparse gradients preserve  $>80\%$  directional alignment with the exact gradient. Cosine similarity increases monotonically with  $k$  ( $0.82 \rightarrow 0.85 \rightarrow 0.89$  for  $k=4, 8, 16$  post-shift), consistent with the flat recovery curve: most directional information is captured by the first few paths.

What property of gradient-based training produces and maintains this near-isotropy remains an open question. Dynamical isometry theory shows that orthogonal initialization can produce near-uniform singular values at  $t=0$ , and edge-of-chaos results show that training drives the spectral radius toward 1, but neither explains why the *full* spectrum remains near-uniform throughout training rather than developing large outlier singular values. Tanh saturation may act as a soft equalizer (neurons driven toward saturation by large singular value modes have derivatives near zero, selectively dampening the dominant modes), but this mechanism has not been formalized.

This connects to random projection theory [Johnson and Lindenstrauss, 1984]: random projections preserve distance structure most reliably when the source distribution is isotropic, because the projection error is uniform across all directions. The near-isotropy of the Jacobian is precisely the condition under which random subsampling is most robust. The condition numbers on Lorenz ( $2.95 \pm 0.36$  at  $n=64$ ) are actually lower than on sine ( $3.97 \pm 0.81$ ), indicating that the more variable recovery on chaotic dynamics reflects numerical instability of the Jacobian *magnitude* rather than degraded isotropy.

## 5.2 Architecture-Dependent Redundancy Thresholds

The cross-architecture comparison (Table 14) reveals that gradient transport redundancy is a general phenomenon, but the degree of redundancy varies by architecture.

Table 14: Gradient transport redundancy across architectures. The threshold for  $>70\%$  recovery varies from  $\sim 6\%$  (RNNs) to  $\sim 33\%$  (transformers), reflecting different specialization structures. Transformer threshold measured with sparse gradient transport (Section 4.7).

Architecture	Transport unit	Threshold	Recovery at threshold	Degenerate
Vanilla RNN	Neuron	$k=4/64$ (6%)	$84 \pm 6\%$	$k=0$ (fails)
LSTM	Gate Jacobian	$k=4/64$ (6%)	$\geq 100\%$	$k=0$ (fails)
Transformer	Attention head	$k=4-6/12$ (33-50%)	$77-107\%^\dagger$	$k=1$ (0%)

<sup>†</sup> $k=4$  is borderline (high seed variance);  $k=6$  is robust (107% recovery, 3 seeds).

In RNNs, the near-isotropic Jacobian (condition numbers 2.6–6.5) means all neurons carry similar sensitivity information. Any small random subset provides a representative gradient estimate. The threshold is correspondingly low: 4 of 64 neurons, regardless of which 4 (Section 4.3).

In transformers, the mechanism is different: heads are functionally specialized (Section 4.7), so gradient signal is concentrated rather than uniformly distributed. The Fisher head selection experiment (Section 4.8) confirms this with a +24.3pp oracle–anti gap across 5 seeds (vs.  $-0.6$ pp in RNNs), while entropy-based selection matches random. The threshold is correspondingly higher:  $\sim 33\%$  of heads for gradient-only sparsity, or  $\sim 50\%$  when forward-pass corruption is also present. The threshold difference is confounded with the number of transport units: in absolute terms, both architectures require  $k \approx 4$ . Disentangling the effects of unit count and unit specialization would require testing transformers with substantially more heads (e.g., 64) at fixed  $k$ .

We emphasize that these are analogous phenomena under a shared framing (gradient transport redundancy), not the same mechanism in different architectures: the RNN result concerns forward-mode Jacobian propagation redundancy, while the transformer result concerns backward-mode gradient transport through attention heads. Despite these quantitative and mechanistic differences, the qualitative pattern is similar across all three architectures: (1) a degenerate baseline where gradient transport is eliminated or near-eliminated collapses completely, (2) there exists a threshold above which recovery is substantial ( $>70\%$ ), and (3) below this threshold, performance degrades rapidly. The existence of a redundancy threshold holds across all three architecture families tested; the threshold level is architecture-specific and predictable from the specialization structure of the transport units.

## 5.3 Implicit Regularization on Chaotic Dynamics

On the Lorenz attractor (Section 4.2), sparse Jacobian propagation is *more numerically stable* than full RTRL. With 5 seeds, the pattern is clear:  $k=4$  achieves consistent post-shift MSE ( $0.015 \pm 0.002$  at  $n=64$ ,  $CV = 13\%$ ) while full RTRL varies wildly ( $0.036 \pm 0.035$ ,  $CV = 88\%$ ), diverging entirely on 2 of 5 seeds. At  $n=128$ , the instability worsens: full RTRL’s CV reaches 161% and it diverges on 3 of 5 seeds, while  $k=4$  remains tight ( $0.016 \pm 0.001$ ,  $CV = 8\%$ ).

In a chaotic system, nearby trajectories diverge exponentially. Mikhaeil et al. [2022] prove that loss gradients of RNNs producing chaotic dynamics always diverge, regardless of architecture. The RTRL Jacobian tensor inherits this instability: the sensitivity  $\partial h_t / \partial \theta$  grows exponentially with  $t$ , even when the gradient signal it encodes is bounded. Full RTRL propagates this exponential

growth faithfully, injecting multiplicative noise into the gradient. Sparse propagation, by summing over only  $k$  of  $n$  terms per row, implicitly dampens this growth, a form of gradient regularization. The spectral analysis (Table 13) confirms the mechanism: on the seeds where full RTRL diverges, the Jacobian’s condition number exceeds  $10^4$ , indicating catastrophic loss of isotropy. Sparse subsampling avoids amplifying these pathological modes.

This observation connects to a broader point: the “exact” gradient is not always the best gradient. On chaotic dynamics, the exact RTRL gradient is numerically unstable, and approximations that introduce bias can outperform exact methods by reducing variance. UORO’s rank-1 compression achieves an even stronger regularization effect ( $0.0025 \pm 0.0006$  on Lorenz, outperforming all other methods), which explains its advantage on chaotic tasks, at the cost of destroying useful information on non-chaotic tasks (0.049 on multi-sine vs 0.005 for  $k=4$ ).

## 5.4 When Forward-Mode Breaks Down

Experiment 4 (Section 4.4) reveals a scope condition for all RTRL-based methods: without continuous error signal, the Jacobian accumulates numerical drift during ungrounded propagation, and full RTRL becomes the *worst* method, underperforming even eligibility traces. This predicts that RTRL-based methods will degrade on any task with temporally sparse error signals (reinforcement learning with delayed rewards, sequence-to-sequence with decoder-only loss). The Jacobian needs continuous grounding to remain useful, a scope condition not previously identified in the RTRL literature.

## 5.5 Implications for RTRL Approximation Design

Our results suggest a reframing of the design space for RTRL approximations. Prior work has invested significant engineering effort in designing *structured* approximations: graph-based sparsity patterns that follow network topology (SnAp), optimal matrix factorizations that minimize approximation error (OK), architectural constraints that simplify the Jacobian structure (Irie). Each of these methods implicitly assumes that the *choice* of which Jacobian information to retain is critical.

Our selection invariance result (Section 4.3) challenges this assumption. The information in the recurrent Jacobian is so redundant that even adversarial selection, deliberately retaining only the weakest connections, works as well as oracle selection. This does not invalidate prior methods: SnAp, UORO, and OK may offer advantages on tasks and architectures we have not tested. But it does suggest that the engineering effort devoted to structured selection may yield diminishing returns. A practitioner choosing an RTRL approximation should focus on two questions: (1) does it propagate *any* Jacobian information? and (2) can the architecture solve the task? The specific structure of the approximation appears secondary.

## 5.6 Limitations

Our findings are subject to several scope conditions:

- **Architecture:** Experiments 1–4 use a vanilla tanh RNN; Experiment 5 extends to LSTMs on smooth dynamics; Experiment 7 extends to vision transformers on continual image classification. The principle is confirmed across three architecture families, but each with different redundancy thresholds. LSTM RTRL did not converge on chaotic dynamics (Lorenz), consistent with the theoretical results of Mikhaeil et al. [2022]. GRUs remain untested but are structurally similar to LSTMs. State-space models and linear recurrent units have qualitatively different Jacobian structure and may not exhibit the same isotropy. The transformer

experiment uses a relatively small model (4 blocks, 12 heads); whether the  $\sim 33\%$  gradient-only threshold holds for large-scale transformers with 32+ heads is an open question.

- **Tasks:** RNN experiments evaluate on continuous dynamical prediction with dense error signals; the transformer experiment evaluates on continual image classification with replay (a standard CL benchmark); the BCI experiment (Experiment 9) evaluates on real neural decoding with cross-session electrode drift. Language modeling and reinforcement learning remain untested. Experiment 4 demonstrates that sparse error signals degrade all RTRL variants, establishing a clear boundary. The BCI experiment uses a single session pair from one subject; a full clinical evaluation would require multiple session pairs, multiple subjects, and comparison against standard recalibration baselines.
- **Scale:** We establish the absolute- $k$  scaling law from  $n=64$  to  $n=256$  (Experiment 6), where  $k=4$  at 1.6% of neurons still recovers  $78 \pm 20\%$  of the gap. At  $n=512$ , RTRL itself becomes numerically unstable (the full Jacobian diverges), establishing a practical ceiling for vanilla forward-mode propagation with standard floating-point arithmetic. Networks with  $n > 1000$ , where computational savings would be most impactful, likely require mixed-precision or periodic Jacobian renormalization to remain stable.
- **Seed count:** RNN results (Experiments 1–6, 9) are reported with 5 seeds with mean  $\pm$  s.d.; transformer sparse gradient transport (Experiment 7) uses 3 seeds for the main results (2 additional seeds show compressed dense-trace gaps, consistent with  $k=4$  being borderline); Fisher head selection (Experiment 8) uses 5 seeds; Fisher timing robustness uses 5 seeds. The spectral analysis for Lorenz excludes 2 of 5 seeds where the Jacobian diverged (condition number  $> 10^4$ ); the  $n=256$  spectral analysis uses 3 seeds.
- **Evaluation angle:** Online adaptation to distribution shifts is a novel evaluation protocol that directly tests temporal credit assignment. However, it lacks established baselines in the RTRL literature, making direct comparison with published results difficult. We mitigate this by including standard benchmarks in Experiment 4, where the comparison reveals the architecture rather than the gradient method as the bottleneck.
- **Optimizer:** All main RNN experiments use the Adam optimizer. An SGD ablation on the sine task ( $n=64$ , 5 seeds) confirms the finding is optimizer-independent:  $k=4$  achieves  $92 \pm 1\%$  log recovery under SGD (per-seed: 91.0%, 93.5%, 93.1%, 91.3%, 90.8%), with low variance. Gradient magnitude diagnostics show the median  $k=4/k=64$  gradient ratio is  $\approx 1.0$  for both Adam and SGD, meaning sparse gradients are the same magnitude as full RTRL gradients and Adam’s per-parameter normalization is not compensating for any magnitude reduction. However, SGD is tested on one task only; broader SGD validation remains future work.

## 6 Related Work

**Exact RTRL.** Real-time recurrent learning [Williams and Zipser, 1989] computes exact forward-mode gradients by maintaining the full Jacobian tensor. Its  $O(n^4)$  per-step cost has historically limited it to small networks, motivating the approximation methods below. Recent work by Irie et al. [2024] achieves exact RTRL at  $O(n^2)$  for element-wise recurrent architectures, demonstrating that the cost barrier can be broken by architectural design, at the expense of removing inter-neuron recurrence. Our LSTM results (Section 4.5) suggest an alternative: for standard LSTMs, sparse gate Jacobian propagation achieves most of full RTRL’s benefit without architectural modification.

**Dropping the Jacobian.** At the other extreme, RFLO [Murray, 2019] and e-prop [Bellec et al., 2020] drop the Jacobian propagation term entirely, retaining only the immediate (one-step) derivatives. This is equivalent to our  $k=0$  baseline (eligibility traces). These methods are biologically motivated and computationally cheap ( $O(n^2)$ ), but our results confirm that they fail to adapt to distribution shifts, precisely because they lose the recurrent component of the gradient that carries information across time steps.

**Structured Jacobian approximations.** Between these extremes, several methods approximate the Jacobian propagation with specific structural assumptions. UORO [Tallec and Ollivier, 2018] maintains a rank-1 approximation of the Jacobian, achieving  $O(n^2)$  cost with high variance. Our comparison (Section 4.2) shows this variance is task-dependent: beneficial on chaotic dynamics (where the exact Jacobian is pathological) but destructive on non-chaotic tasks. Benzing et al. [2019] derive an optimal Kronecker-sum approximation (OK) that matches BPTT on Penn Treebank at  $O(n^3)$  cost, below full RTRL’s  $O(n^4)$  but above  $O(n^2)$  methods. Marschall et al. [2020] provide a unified taxonomy of RTRL approximation methods, placing all of the above on a spectrum from exact to maximally approximate.

**SnAp: graph-structured sparsity.** The closest prior work to ours is SnAp [Menick et al., 2021], which also sparsifies the Jacobian propagation. However, SnAp and our approach differ in mechanism, scope, and implications. SnAp uses *graph-structured* sparsity: for a weight-sparse RNN, each neuron propagates Jacobian information only through neurons reachable within  $s$  steps in the weight graph (SnAp- $s$ ). The sparsity pattern is deterministic and topology-dependent; it follows the network’s learned connectivity structure. This requires the network weights themselves to be sparse, an architectural constraint.

In contrast, we keep  $W_{hh}$  fully dense and sparsify only the Jacobian propagation using a random subset of connections that bears no relation to network topology. Our sparsity pattern is random and topology-independent. The key insight from our selection invariance experiment (Section 4.3) is that SnAp’s careful graph-structured selection may be unnecessary: random selection works equally well, and even adversarial selection cannot degrade performance, because the Jacobian is redundant. This prediction (that random sparsity matches structured sparsity for dense-weight RNNs) is testable in SnAp’s framework and represents a concrete contribution to the understanding of Jacobian approximation.

SnAp operates on GRU architectures and evaluates on binary copy and WikiText-2, while we use vanilla tanh RNNs on continuous dynamical tasks. Direct numerical comparison is therefore not possible, but the mechanistic distinction is clear: SnAp’s contribution is a specific structured approximation; our contribution is evidence that the structure is unnecessary.

**Diagonal and linear recurrences.** Zucchet et al. [2023] combine linear recurrent units (LRUs) with RTRL, exploiting the diagonal recurrence structure to reduce cost. This architectural approach eliminates the inter-neuron Jacobian entirely by design, rather than approximating it. Wang et al. [2026] exploit a different form of natural sparsity: in spiking neural networks, biological activity sparsity (most neurons are silent at any given time) makes the Jacobian inherently sparse, enabling linear-memory online learning at whole-brain scale. In contrast, our networks have dense activations; the Jacobian is dense and full-rank, yet redundant. The sparsity we exploit is not in the Jacobian itself but in how much of it needs to be *propagated*.

**Sparse gradient transport in transformers.** Our sparse gradient transport (Section 4.7) detaches non-selected attention heads from the computation graph during backpropagation, restricting gradient flow to  $k$  of  $H$  heads while maintaining the full forward pass. This is distinct from dropout (which zeroes activations in the forward pass for regularization), DropHead [Zhou et al., 2020] (which applies structured dropout to attention heads during training), and head pruning [Voita et al., 2019, Michel et al., 2019] (which identifies and removes redundant heads). Our method tests whether gradient transport through *all* heads is necessary during training, isolating the gradient information question from forward-pass effects. Concurrently, Guo and Sheridan [2026] show that gradient-norm-based head scoring outperforms attention entropy for post-training pruning, a parallel finding to our Experiment 8 result (Fisher/gradient importance  $>$  entropy) in an independent context, suggesting that gradient-based head importance generalizes across the training-time/inference-time divide. The finding that  $\sim 33\%$  of heads suffice for  $>70\%$  recovery, combined with the Fisher head selection result (Section 4.8), establishes that transformer heads are functionally specialized for gradient transport, a structural property not addressed by the pruning literature, which focuses on inference-time redundancy rather than training-time gradient information.

## 7 Conclusion

Gradient transport in neural networks is massively redundant. In RNNs trained online on continuous dynamical prediction, propagating sensitivity through a random 1.6–6% of Jacobian paths recovers 78–84% of full RTRL’s adaptation ability. This redundancy is robust across 5 seeds on simple and chaotic dynamics, across network sizes from  $n=64$  to  $n=256$ , across selection strategies (including adversarial), and across recurrent architectures (vanilla tanh RNNs and LSTMs). On chaotic dynamics, sparse propagation is not only effective but more numerically stable than full RTRL:  $k=4$  maintains a coefficient of variation of 8–13% across seeds, while full RTRL’s CV reaches 88–161%, diverging on 2–3 of 5 seeds. The principle extends to transformers: sparse gradient transport through 50% of attention heads *outperforms* the dense reference via implicit regularization, with 33% as a borderline threshold (high seed variance). Fisher-guided head selection confirms the mechanism: a +24.3pp Fisher oracle–anti gap across 5 seeds (vs.  $-0.6$ pp in RNNs) shows transformer heads are specialized while RNN neurons are isotropic, and entropy-based selection matching random rules out dormancy as the explanation. On real primate neural data, sparse RTRL ( $k=4$ ) adapts online to cross-session electrode drift spanning 7 months ( $80 \pm 11\%$  recovery, 5 seeds), with the stability advantage over full RTRL reproducing on biological signals.

The critical transition is binary: from no gradient transport (eligibility traces for RNNs, single-head for transformers) to transport above an architecture-dependent threshold. Below the threshold, learning collapses; above it, recovery is substantial. The threshold varies ( $\sim 6\%$  of neurons for RNNs,  $\sim 33\%$  of heads for transformers), reflecting different degrees of specialization in the transport units. But its existence holds across all three architecture families tested. Spectral analysis reveals the mechanism in RNNs: the Jacobian tensor is full-rank but near-isotropic, so any random subset provides a directionally representative gradient estimate.

Perhaps the most practically significant finding is the absolute- $k$  scaling law:  $k=4$  Jacobian paths suffice regardless of network size, from  $n=64$  (6%) to  $n=256$  (1.6%). This means sparse RTRL’s computational advantage grows with scale: at  $n=256$ , it propagates  $64\times$  less Jacobian information than full RTRL while  $k=4$  post-shift MSE remains tight ( $0.0038 \pm 0.0008$ ), even as full RTRL shows  $22\times$  seed-dependent variance. RTRL’s numerical instability establishes the practical ceiling at  $n \approx 256$ –512.

These results suggest a reframing of the design space for gradient transport approximations. Prior work has focused on structured approximation schemes (specific factorizations, specific sparsity patterns, specific architectural constraints), implicitly assuming that *which* gradient information to retain is a critical design choice. For RNNs, our findings suggest it is not: the bottleneck is having sufficient gradient transport at all, and the structure of that transport is secondary. For transformers, selection matters more due to head specialization, but the existence of a redundancy threshold (below which learning collapses and above which recovery is substantial) holds across all architectures tested.

We also identify a failure mode of forward-mode sensitivity propagation that applies broadly: without continuous error signal to ground the Jacobian, extended propagation produces gradient estimates worse than no propagation at all. This scope condition (that RTRL methods require dense error feedback) has not been explicitly characterized in prior work and constrains the applicability of the entire family of forward-mode approaches.

**Future work.** Three directions are most pressing. First, scaling sparse gradient transport to transformers with 32+ heads would test whether the  $\sim 33\%$  threshold decreases with more heads (as it does for RNN neurons) or remains constant, disentangling the effects of unit count and specialization. Second, extending to language modeling and reinforcement learning would test whether gradient transport redundancy holds under different loss structures and sequence statistics. Third, developing a formal theoretical bound connecting Jacobian isotropy to gradient direction error (as a function of  $k$ ,  $n$ , and the condition number) would place these empirical findings on rigorous theoretical ground. On the applied side, the BCI cross-session result (Section 4.9) motivates a full clinical evaluation: multiple session pairs at varying time gaps, multiple subjects, and comparison against standard recalibration methods, potentially enabling continuous decoder adaptation without manual recalibration.

## References

- Guillaume Bellec, Franz Scherr, Anand Subramoney, Elias Hajek, Darjan Salaj, Robert Legenstein, and Wolfgang Maass. A solution to the learning dilemma for recurrent networks of spiking neurons. *Nature Communications*, 11(1):3625, 2020.
- Frederik Benzing, Marcelo Matheus Gauy, Asier Mujika, Anders Martinsson, and Angelika Steger. Optimal kronecker-sum approximation of real time recurrent learning. In *International Conference on Machine Learning*, pages 604–613. PMLR, 2019.
- Alexey Dosovitskiy, Lucas Beyer, Alexander Kolesnikov, Dirk Weissenborn, Xiaohua Zhai, Thomas Unterthiner, Mostafa Dehghani, Matthias Minderer, Georg Heigold, Sylvain Gelly, Jakob Uszkoreit, and Neil Houlsby. An image is worth 16x16 words: Transformers for image recognition at scale. In *International Conference on Learning Representations*, 2021.
- Yuxi Guo and Paul Sheridan. Greedy-gnorm: A gradient matrix norm-based alternative to attention entropy for head pruning. *arXiv preprint arXiv:2602.04491*, 2026.
- Sepp Hochreiter and Jürgen Schmidhuber. Long short-term memory. *Neural Computation*, 9(8):1735–1780, 1997.
- Kazuki Irie, Anand Gopalakrishnan, and Jürgen Schmidhuber. Exploring the promise and limits of real-time recurrent learning. In *International Conference on Learning Representations*, 2024.

- William B Johnson and Joram Lindenstrauss. Extensions of Lipschitz mappings into a Hilbert space. *Contemporary Mathematics*, 26:189–206, 1984.
- Joseph G Makin, Joseph E O’Doherty, Mariana M F Cardoso, and Philip N Sabes. Superior arm-movement decoding from cortex with a new, unsupervised-learning algorithm. *Journal of Neural Engineering*, 15(2):026010, 2018.
- Owen Marschall, Kyunghyun Cho, and Cristina Savin. A unified framework of online learning algorithms for training recurrent neural networks. *Journal of Machine Learning Research*, 21(135):1–34, 2020.
- Jacob Menick, Erich Elsen, Utku Evci, Simon Osindero, Karen Simonyan, and Alex Graves. A practical sparse approximation for real time recurrent learning. In *International Conference on Learning Representations*, 2021.
- Paul Michel, Omer Levy, and Graham Neubig. Are sixteen heads really better than one? In *Advances in Neural Information Processing Systems*, volume 32, 2019.
- Jonas M Mikhaeil, Zahra Monfared, and Daniel Durstewitz. On the difficulty of learning chaotic dynamics with RNNs. In *Advances in Neural Information Processing Systems*, volume 35, 2022.
- James M Murray. Local online learning in recurrent networks with random feedback. *eLife*, 8:e43299, 2019.
- Joseph E O’Doherty, Mariana M B Cardoso, Joseph G Makin, and Philip N Sabes. Nonhuman primate reaching with multichannel sensorimotor cortex electrophysiology, 2017.
- Corentin Tallec and Yann Ollivier. Unbiased online recurrent optimization. In *International Conference on Learning Representations*, 2018.
- Ashish Vaswani, Noam Shazeer, Niki Parmar, Jakob Uszkoreit, Llion Jones, Aidan N Gomez, Lukasz Kaiser, and Illia Polosukhin. Attention is all you need. In *Advances in Neural Information Processing Systems*, volume 30, 2017.
- Elena Voita, David Talbot, Fedor Moiseev, Rico Sennrich, and Ivan Titov. Analyzing multi-head self-attention: Specialized heads do the heavy lifting, the rest can be pruned. In *Proceedings of the 57th Annual Meeting of the Association for Computational Linguistics*, pages 5797–5808, 2019.
- Chaoming Wang, Xingsi Dong, Zilong Ji, Mingqing Xiao, Jiedong Jiang, Xiao Liu, Yuxiang Huan, and Si Wu. Model-agnostic linear-memory online learning in spiking neural networks. *Nature Communications*, 17(1745), 2026.
- Paul J Werbos. Backpropagation through time: what it does and how to do it. *Proceedings of the IEEE*, 78(10):1550–1560, 1990.
- Ronald J Williams and David Zipser. A learning algorithm for continually running fully recurrent neural networks. *Neural Computation*, 1(2):270–280, 1989.
- Friedemann Zenke, Ben Poole, and Surya Ganguli. Continual learning through synaptic intelligence. In *International Conference on Machine Learning*, pages 3987–3995. PMLR, 2017.
- Wangchunshu Zhou, Tao Ge, Ke Xu, Furu Wei, and Ming Zhou. Scheduled drophead: A regularization method for transformer models. In *Findings of EMNLP*, 2020.

Nicolas Zucchet, Robert Meier, Simon Schug, Asier Mujika, and João Sacramento. Online learning of long-range dependencies. In *Advances in Neural Information Processing Systems*, volume 36, 2023.